Atmos. Chem. Phys., 25, 3669–3685, 2025
https://doi.org/10.5194/acp-25-3669-2025


Atmospheric Chemistry and Physics
Open Access
EGU



# Measurement report: The variation properties of aerosol hygroscopic growth related to chemical composition during new particle formation days in a coastal city of Southeast China

**Lingjun Li[1,2,3], Mengren Li[1,2,3], Xiaolong Fan[1,2,3], Yuping Chen[1,2,3], Ziyi Lin[1,2,3], Anqi Hou[1,2], Siqing Zhang[1,2,3], Ronghua Zheng[1,2,3], and Jinsheng Chen[1,2,3]**

[1]Institute of Urban Environment, Chinese Academy of Sciences, Xiamen 361021, China
[2]Fujian Key Laboratory of Atmospheric Ozone Pollution Prevention, Institute of Urban Environment, Chinese Academy of Sciences, Xiamen 361021, China
[3]College of Resources and Environment, University of Chinese Academy of Sciences, Beijing 100086, China

**Correspondence:** Mengren Li (mrli@iue.ac.cn) and Jinsheng Chen (jschen@iue.ac.cn)

Received: 26 July 2024 – Discussion started: 18 September 2024
Revised: 14 January 2025 – Accepted: 28 January 2025 – Published: 27 March 2025

**Abstract.** The scattering of solar radiation by aerosol is significantly affected by relative humidity (RH) due to the aerosol hygroscopicity. In order to better understand the characteristics of aerosol scattering hygroscopic growth and its influencing factors during new particle formation (NPF) days, we conducted an in situ campaign from February to April 2022 in Xiamen, a coastal city in Southeast China. The aerosol scattering hygroscopic growth factor $f(\mathrm{RH})$, commonly used to describe the aerosol indirectly hygroscopicity, varies greatly due to the influence of aerosol chemical composition and size. In the relatively clean atmosphere of Xiamen, NPF events occur frequently, and the variation in chemical composition during events has a substantial influence on the aerosol scattering hygroscopic growth. In this study, we investigated the features and influencing factors of $f(\mathrm{RH})$ on the NPF days. The research results emphasized that $f(\mathrm{RH})$ differed significantly between NPF and non-NPF days, mainly impacted by the aerosol chemical compositions, especially sulfate and nitrate. On NPF days, sulfate was the dominant contributor to $f(\mathrm{RH})$, distinguishing it from the non-NPF days. Aerosol hygroscopicity–chemical composition closure demonstrated that $NH_4HSO_4$ was the main driving force (30.78 %) of the hygroscopicity parameter $\kappa_{f(\mathrm{RH})}$ when NPF events happened, while $NH_4NO_3$ played a dominant role in $\kappa_{f(\mathrm{RH})}$ (up to 35 %) for non-NPF days. Although the uncertainty of the organic aerosol (OA) to hygroscopicity might exist due to the varieties of chemical components and oxidation level, it was the crucial driving factor for the variation in aerosol hygroscopicity. The findings of this study would be helpful for the further understanding of the properties of aerosol hygroscopicity in the coastal area, and it would complement the hygroscopic growth factors in the models of air quality and climate change.

## 1 Introduction

Atmospheric aerosols have direct and indirect effects on atmospheric visibility, the earth–atmosphere radiation budget, clouds, and precipitation, which in turn affect climate (Charlson et al., 1992); these effects are strongly dependent on the hygroscopic properties of the ambient aerosol and the relative humidity (RH). The aerosol optical properties are key parameters for accurately estimating the direct radiative forcing caused by aerosols in climate models (IPCC, 2021). The aerosol hygroscopicity has a significant impact on the optical properties by altering particle size and refractive index and ultimately on the climatic and environmental effects of aerosols (Covert et al., 1972; Tang, 1996; Malm and Day,

2001). Particles absorb water through hygroscopic growth, growing to sizes that are more efficient for light scattering, and their refractive index changes, resulting in enhanced aerosol scattering (Seinfeld et al., 1998). The aerosol liquid water content (ALWC) increases as particles absorb water in humid environments due to aerosol hygroscopicity. The condensed water in aerosols serves as an effective medium for multiphase chemistry, promoting the transformation of active gaseous pollutants into particles. Meanwhile, the newly formed hygroscopic aerosol components, such as secondary aerosols, can also alter aerosol hygroscopic behaviors and enhance aerosol extinction efficiency. These processes lead to regional visibility impairment and accelerated formation of heavy haze. Therefore, aerosol hygroscopicity can profoundly affect atmospheric chemical processes (Wu et al., 2018) and air quality (Liu et al., 2020a).

Aerosol hygroscopic growth becomes the main factor affecting the aerosol optical properties at high ambient humidity due to the enhanced aerosol hygroscopicity and increased RH (Jin et al., 2022). The aerosol scattering hygroscopic growth factor ($f(\mathrm{RH})$) is defined as the ratio of aerosol scattering coefficient at an elevated RH level ($\sigma_{sp}(\mathrm{RH}, \lambda)$) to that under dry conditions ($\sigma_{sp}(\mathrm{RH_{dry}}, \lambda)$) (usually $\mathrm{RH} < 40\,\%$) at a given wavelength. The scattering enhancement owing to hygroscopic growth strongly depends on the source of the aerosol, which varies in chemical composition (Yan et al., 2009; Sheridan et al., 2002; Fierz-Schmidhauser et al., 2010b; Kotchenruther and Hobbs, 1998). For example, marine aerosols tend to have higher $f(\mathrm{RH})$ than urban or continental aerosols, and their $f(\mathrm{RH})$ decreases under strong anthropogenic influence (Zieger et al., 2010; Yan et al., 2009; Sheridan et al., 2001). Mineral dust and freshly emitted biomass combustion aerosols exhibit the lowest $f(\mathrm{RH})$ values among the aerosol types studied (Sheridan et al., 2002; Pan et al., 2009; Fierz-Schmidhauser et al., 2010b). Hydrophilic species such as secondary inorganic components, sea salts, and water-soluble organics in the aerosol are the main contributors to the hygroscopic growth (Li et al., 2021; Fierz-Schmidhauser et al., 2010b), while black carbon and some organic carbons are the major proportion of the hydrophobic species (Liu and Zhang, 2010). Thus, discrepancies in the chemical composition of the aerosol, the fraction of soluble and insoluble chemical components, lead to variations in $f(\mathrm{RH})$ (Malm et al., 2005; Zieger et al., 2014; Zhang et al., 2015). Additionally, particle number size distribution (PNSD) is another factor affecting $f(\mathrm{RH})$. For a fixed chemical composition, $f(\mathrm{RH})$ decreases with increasing particle size (Fierz-Schmidhauser et al., 2010a; Zieger et al., 2010; Baynard et al., 2006). Particle morphology, including shape and mixing state, significantly affects aerosol hygroscopicity. Giordano et al. (2015) demonstrated that not only does the non-spherical shape of particles influence their hygroscopic behavior, but also changes in the mixing state of particles – whether they are internally or externally mixed – influence their hygroscopic properties (Stevens and Dastoor, 2019). Note that the aerosol chemical compositions, particle sizes, and morphology have a combined impact on $f(\mathrm{RH})$ in the atmospheric environment, as the three are closely related (Wu et al., 2017; Kreidenweis and Asa-Awuku, 2014).

The observation site is situated in Xiamen, a fast-urbanization coastal city in Southeast China, at the junction of land and sea. As a result of massive population growth and rapid economic development, its atmospheric environment is subjected to complex pollution situations, such as increased atmospheric oxidation (Liu et al., 2022) and relatively high nitrogen oxide pollution (Chen et al., 2023). Notably, despite these conditions, aerosol concentrations remain generally lower compared to those in highly polluted megacities in China, according to open-access data from the China National Environmental Monitoring Centre (https://www.zq12369.com/index.php, last access: 2 November 2024). On the other hand, it is located in a subtropical city with relatively high air temperatures and high RH. High RH not only directly increases light scattering, leading to the decline of visibility (Won et al., 2021), but also affects the aerosol chemical processes involved in the particle formation (Sun et al., 2013; Chen et al., 2021). New particle formation (NPF) events occur frequently in this coastal city in Southeast China with relatively clean air quality (Wang et al., 2022). NPF is a process in which low-volatile compounds emitted from natural or anthropogenic sources form into thermodynamically stable molecular clusters and grow into larger particles via condensation or collision with other vapors or particles (Holmes, 2007). When NPF occurs, both the PNSD and the chemical composition of the aerosol undergo significant changes, which have a remarkable influence on the aerosol hygroscopicity and $f(\mathrm{RH})$. Previous studies of $f(\mathrm{RH})$ had been conducted mainly in the megacity agglomerations such as the North China Plain, the Yangtze River Delta, and the Pearl River Delta (Liu et al., 2012; Xia et al., 2019; Ding et al., 2021; Jin et al., 2022; Zhao et al., 2019a), while limited attention had been paid to southeastern coastal areas with relatively low levels of particles and high RH. Meanwhile, these studies have focused more on the effect of aerosol chemical composition on $f(\mathrm{RH})$ (Li et al., 2021; Wang et al., 2021; Jin et al., 2022); however, the exploration of the variation in $f(\mathrm{RH})$ during NPF days is quite limited in China.

In order to investigate the characteristics of $f(\mathrm{RH})$ and its influencing factors during NPF days, enhanced observations utilized a high-resolution humidified nephelometer system combined with PNSD instruments to measure $f(\mathrm{RH})$ for RH ranging from 40 % to 91 % in urban Xiamen. Routine measurements including other aerosol chemical and physical properties were also synchronously conducted. Differences and variations in $f(\mathrm{RH})$ between NPF and non-NPF days were explored, and the effects of aerosol chemical compositions on $f(\mathrm{RH})$ were also discussed. The research was expected to characterize the properties of aerosol hygroscopicity during NPF and non-NPF days in the coastal area with

relatively low levels of particles and high RH and provide references to the model improvement for air quality and climate change.

## 2 Instruments and methods

### 2.1 Observation site

The enhanced observations were carried out at the Institute of Urban Environment of the Chinese Academy of Sciences in Xiamen (IUE, CAS), which is situated on the west coast of the Taiwan Strait. The observation station (118°03′ E, 24°36′ N) was located on the roof of an 80 m tall building, a typical urban site surrounded by two main trunk roads (Jimei main road and Haixiang express road), shopping malls, educational institutions, and residential areas, and there were no apparent industrial emission sources nearby. Thus, the collected data can accurately represent the average air quality levels in the urban area of Xiamen. The observations were conducted consecutively from 1 February to 30 April 2022.

### 2.2 Observation instruments

The $f(\mathrm{RH})$ values were obtained using a multi-band dual-nephelometer system (PB-FRH100, BMET, China) comprising a nephelometer for aerosol scattering coefficients under dry conditions and another nephelometer for humidified aerosols. The airflow initially passed through two tandem Nafion dryers which could decrease the RH of the airflow to less than 30 %. After this, the airflow was divided into two routes: one was directed straight into the nephelometer, while the other was humidified via a Gore-Tex tube set in a stainless-steel tube before flowing into the nephelometer. The space between these two tubes contained circulating water, which was heated by two water baths. The scattering coefficients of dry and humidified $PM_{2.5}$ were measured at three wavelengths (450, 525, and 635 nm) using two nephelometers. The detailed principles and operation of the system are described in the Supplement (Sect. S1). This study set the minimum and maximum RH at 40 % and 91 %, respectively, with a 45 min cycle for humidification.

An integrating nephelometer (Aurora-3000, Ecotech, Australia) was used to simultaneously and continuously measure the 5 min average $\sigma_{sp}$ at the same three wavelengths, and the $\sigma_{sp}$ at 525 nm was appropriate for characterizing the aerosol scattering coefficient in this study. A scanning mobility particle sizer (SMPS, model 3938 L50, TSI Inc., USA), integrated with a differential mobility analyzer (DMA, model 3082, TSI Inc., USA); a butanol-based condensation particle counter (CPC, model 3750, TSI Inc., USA); and an aerosol neutralizer were used to continuously measure the PNSD in the range of 7–300 nm over a 5 min scanning interval during the measurement. The hourly chemical composition of aerosol, including sulfate ($SO_4$), nitrate ($NO_3$), ammonium ($NH_4$), chloride (Chl), and organics (Org), was measured by a high-resolution Aerodyne Aerosol Chemical Speciation Monitor (Q-ACSM). The relative ion efficiency (RIE) for $SO_4$, $NO_3$, $NH_4$, Chl, and Org was 0.53, 1.1, 5.49, 1.3, and 1.4, respectively. PMF/ME-2 models were performed to identify organic aerosol (OA) factors resolving primary organic aerosol (POA) and secondary organic aerosol (SOA) in this study. POA is the unoxygenated component, and SOA is a more oxygenated organic aerosol. More detailed descriptions on the PMF analysis are given in Sect. S2. An AE-31 Aethalometer (Magee Scientific, USA) was used to measure the black carbon (BC) aerosol concentrations. Hourly mass concentrations of $PM_{2.5}$ and $PM_1$ were measured by a tapered element oscillating microbalance (TEOM1405, Thermo Scientific Corp., USA). Ambient meteorological parameters, including air temperature ($T$), RH, wind speed (WS), and wind direction (WD), were continuously monitored by an ultrasonic weather station instrument (150WX, Airmar, USA). Gaseous pollutants (carbon oxide, sulfur dioxide, and nitrogen dioxide) were measured by online Thermo Scientific instruments TEI 48i, 49i, 43i, and 42i (Thermo Scientific Corp., USA).

### 2.3 Identification and classification of new particle formation

The NPF process involves nucleating and growing. The particles nucleated at a critical size of approximately $1.5 \pm 0.4$ nm (Kulmala et al., 2012) and then could grow into larger particles. During the sampling period, a total of 85 d of valid observations was available for PNSD analysis. The particles were divided into three modes: nucleation mode ($< 25$ nm), Aitken mode (25–100 nm), and accumulation mode ($> 100$ nm) in this study (Kalkavouras et al., 2021; Shen et al., 2022; Wang et al., 2022). To identify NPF events, the visual analysis of PNSD data described by Dal Maso et al. (2005) was used. If a new particle mode is observed in the nucleation mode within a few hours and the mode shows clear signs of growth, characterized by a distinct "banana" shape in the time series of PNSD, then the day can be classified as an NPF event day. With the exception of NPF days, all other days are classified as non-NPF days or undefined days. Non-NPF days are confirmed when there is clearly no evidence of NPF or when the above criteria are not met. Besides, days that cannot fulfill the criteria to be identified as NPF or non-NPF days were classified as undefined days, and they are characterized by the presence of some particles in the nucleation mode with no visible signs of growth or by the observation of growth not in the nucleation mode.

### 2.4 Data processing

The scattering Ångström exponent ($\alpha$) indicates the wavelength dependence of aerosol scattering, and the parameters related to aerosol size are relatively low for large particles and relatively high for small particles (Guan et al., 2021). It

is expressed as follows:

$$\alpha = \frac{\log\left(\sigma_{sp,\lambda_1}\right) - \log(\sigma_{sp,\lambda_2})}{\log(\lambda_1) - \log(\lambda_2)}, \quad (1)$$

where $\lambda_1 = 450$ nm and $\lambda_2 = 635$ nm in this study.

The overall hygroscopicity parameter $\kappa_{f(\mathrm{RH})}$ can be obtained from the measured $f(\mathrm{RH})$. The detailed calculation procedure of this method is shown in Supplement (Sect. S3).

For the calculation of the hygroscopicity parameter $\kappa$ based on the measured aerosol chemical composition data, we used the mass concentrations of OA, $SO_4^{2-}$, $NO_3^-$, $NH_4^+$, and $Cl^-$ provided by the ACSM. In this study, a simplified ion-pairing scheme proposed by Gysel et al. (2007) was used to obtain the concentrations of AN, AS, ABS, and AC by turning mass concentrations of ions into mass concentrations of the corresponding inorganic salts. The $\kappa$ values and densities of these salts are shown in Table S1 in the Supplement (Liu et al., 2014; Wu et al., 2016; Kuang et al., 2020). The simple mixing rule, called Zdanovskii–Stokes–Robinson (ZSR), is commonly used in $\kappa_{\mathrm{chem}}$ calculations; therefore, the $\kappa_{\mathrm{chem}}$ of this study can be calculated on the basis of chemical volume fractions $\varepsilon_i$ (Petters and Kreidenweis, 2007) (see Sect. S4 for a detailed process).

## 3 Results and discussion

### 3.1 Overview of $f(\mathrm{RH})$ and derived aerosol variables observations

The typical levels of light-scattering coefficients ($\sigma_{sp}$), $f(\mathrm{RH})$ values at RH = 80 % ($f(80\,\%)$), scattering Ångström exponents ($\alpha$), $PM_{2.5}$ mass concentrations, and ambient RH from February to April 2022 are displayed in Fig. S3 in the Supplement. To evaluate the aerosol hygroscopicity conveniently, $f(80\,\%)$ was often employed (Xia et al., 2023, 2019; Zhao et al., 2019b; Wu et al., 2017). The scattering hygroscopic growth factor $f(80\,\%)$ ranged from 1.00 to 2.48, with an average factor of $1.44 \pm 0.15$ during the whole campaign. The mean concentration of $PM_{2.5}$ was $24.79 \pm 17.74\ \mu g\ m^{-3}$, suggesting the $PM_{2.5}$ pollution was relatively low in Xiamen, referring to the air quality index (AQI) grading standard of China ($PM_{2.5} \leq 35\ \mu g\ m^{-3}$). During the period of observation, the hourly mean $\sigma_{sp}$ measured under dry conditions varied from 1.15 to 662.57 $Mm^{-1}$, with a mean of $135.50 \pm 108.78\ Mm^{-1}$, and its maximum occurred at the peak of $PM_{2.5}$ concentrations. The $\alpha$ was usually considered an indicator of particle size, which was high when $PM_{2.5}$ level was low, indicating that there were more fine particles existing in $PM_{2.5}$ with low concentrations. At the same time, the variation trend of $f(80\,\%)$ was similar to that of $\alpha$. Ambient RH fluctuated considerably and was generally at a high level. The wind direction was more evenly distributed, and the wind speed was relatively stable, concentrated at 1–3 $m\ s^{-1}$. The comparison presented in Fig. 1 and Table S2 implies that $f(\mathrm{RH})$ varied widely across different regions,

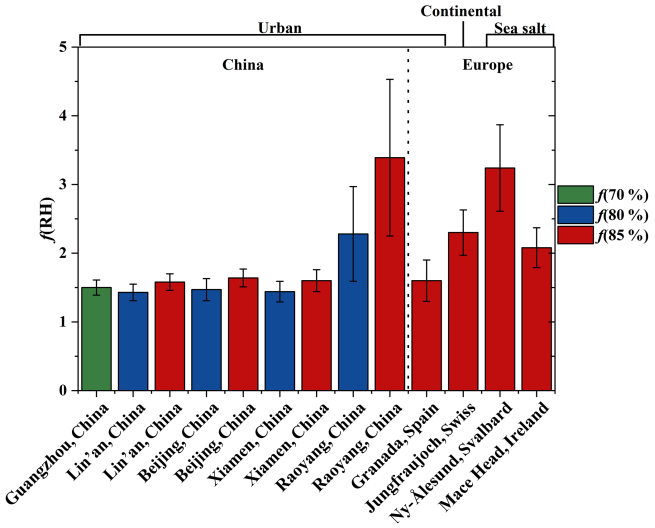


**Figure 1.** Mean values of $f(80\,\%)$, $f(85\,\%)$, and $f(70\,\%)$ at different observation sites. The error bars represent standard deviation. Blue, green, and red represent $f(80\,\%)$, $f(85\,\%)$, and $f(70\,\%)$, respectively.

with consistently higher values observed in Europe compared to China. The differences between $f(\mathrm{RH})$ in this study and in other regions of China were smaller than those outside of China. In urban China (Lin'an, Beijing, Guangzhou, and Xiamen), $f(\mathrm{RH})$ was generally small (Zhang et al., 2015; Zhao et al., 2019b; Ren et al., 2021; Li et al., 2021), whereas in Raoyang, greatly influenced by anthropogenic polluted aerosols, $f(\mathrm{RH})$ raised significantly (Wu et al., 2017). Urban area in Europe (Granada, Spain) also displayed similar values of $f(\mathrm{RH})$ (Titos et al., 2014). Nevertheless, the $f(\mathrm{RH})$ of continental aerosols in Europe (Jungfraujoch, Switzerland) obviously surpassed what had been observed in China (Zieger et al., 2013). In the Arctic (Ny-Ålesund, Svalbard) and the shore of the ocean (Mace Head), $f(\mathrm{RH})$ showed high values due to the sea salt (Zieger et al., 2010, 2013). However, Mace Head, which was also exposed to air pollution from the urban areas, had lower $f(\mathrm{RH})$ than the undisturbed Arctic. Thus, the large variability in $f(\mathrm{RH})$ across measurement sites was primarily attributed to the different aerosol sources and chemical composition.

The entire campaign was divided into three types of days – NPF, undefined, and non-NPF – based on the above classification method. The PNSD spectrum and number concentration of the example NPF and non-NPF days from February to April 2022 are shown in Fig. S4 and Sect. S5. Eleven NPF days were identified, representing approximately 12.94 % of all observed days. In addition, we categorized 18 d as non-NPF days and the remaining days as undefined. The statistical analysis of particle number concentrations on different days during the observation period is summarized in Table S3. The mean number concentrations of nucleation, Aitken, and ac-

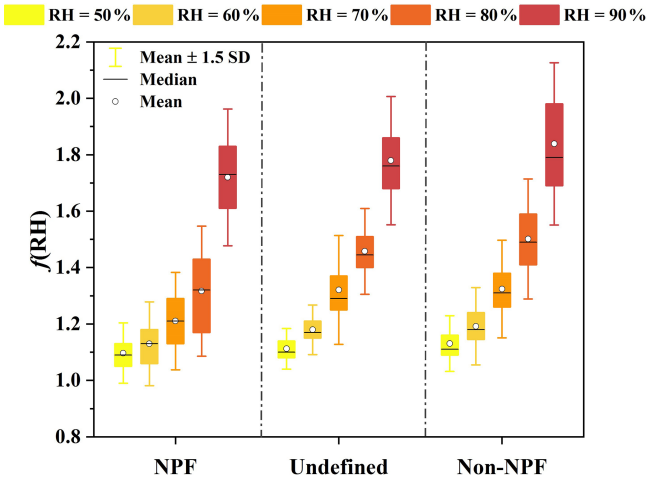


**Figure 2.** The $f(\mathrm{RH})$ measured for a given RH on different days. The $f(\mathrm{RH})$ values at RH = 50 %, 60 %, 70 %, 80 %, and 90 % were counted for the three types of days: NPF, undefined, and non-NPF, respectively. Different colors represent different RH. The error bars represent the mean ± 1.5 standard deviation.

cumulation modes were $1.66 \times 10^3 \pm 1.59 \times 10^3\ \mathrm{cm}^{-3}$, $3.80 \times 10^3 \pm 2.80 \times 10^3\ \mathrm{cm}^{-3}$, and $8.59 \times 10^2 \pm 4.04 \times 10^2\ \mathrm{cm}^{-3}$ on NPF days, contributing 26.25 %, 60.14 %, and 13.61 % to total number concentration, respectively. The majority of particle number concentrations were comprised of nucleation and Aitken mode particles. Figure 2 explores the variations in $f(\mathrm{RH})$ with RH growth on different days. Firstly, $f(\mathrm{RH})$ emerged with an approximately exponential rise as RH increased, with a significant growth when the RH ranged from 80 % to 90 %, the interval of which was the most beneficial to the aerosol scattering hygroscopic growth (Liu et al., 2013). Moreover, Zhao et al. (2019b) found a prominent difference in the aerosol hygroscopicity when RH exceeded 90 %, with aerosol hygroscopicity in this humidity range being lower than when RH was below 90 %. These results indicate that particles exhibited different hygroscopicity behaviors under different RH conditions, which were probably related to the chemical composition, particle size, and morphology of aerosols. Secondly, the characteristics of $f(\mathrm{RH})$ were distinct among different days, especially between NPF days and non-NPF days (Fig. S5). When RH was below 80 %, $f(\mathrm{RH})$ was significantly lower during NPF days compared to non-NPF and undefined days. The $f(\mathrm{RH})$ growth of NPF days was greater than those of the other two sorts of days for RH between 80 % and 90 % and vice versa for RH below 80 %. Such a growth pattern caused the $f(\mathrm{RH})$ of the NPF days to reach a level equivalent to that of the other days as the RH rose to 90 %. Moreover, the fluctuations in $f(\mathrm{RH})$ were larger on the NPF days than on the other two sorts of days, indicating $f(\mathrm{RH})$ on NPF days had a greater dispersion. These results might be related to the dramatic increase in particle number concentrations and variations in chemical composition during the NPF days.

The following discussion will focus on the differences in the aerosol scattering hygroscopic growth and the aerosol hygroscopicity between NPF and non-NPF. As undefined days are in a transitional state, they do not accurately reflect the characteristics of the NPF.

### 3.2 Parameterization of the $f(\mathrm{RH})$

To better characterize the dependence of $f(\mathrm{RH})$ on RH, many different empirical expressions have been applied in previous studies to fit the measurements of $f(\mathrm{RH})$ (Kotchenruther et al., 1999; Kotchenruther and Hobbs, 1998; Gasso et al., 2000; Carrico et al., 2003; Pan et al., 2009; Zieger et al., 2014; Yu et al., 2018). We fitted four commonly used empirical equations to the $f(\mathrm{RH})$ values and compared the results to find that Eq. (2) (Chen et al., 2014) was the most suitable for describing the enhanced scattering caused by the monotonic hygroscopic growth (see Fig. S6 and Sect. S6 for a detailed comparison).

$$f(\mathrm{RH}) = a\left(1 - \frac{\mathrm{RH}}{100}\right)^{-b\left(\frac{\mathrm{RH}}{100}\right)}, \tag{2}$$

where $a$ is a coefficient that reflects the level of $f(\mathrm{RH})$ values, and $b$ is the parameter for the magnitude of scattering enhancement unaffected by RH that quantifies aerosol hygroscopicity to some extent. Higher $f(\mathrm{RH})$ is related to higher $a$ and $b$ values.

The fitted $f(\mathrm{RH})$ curves between NPF and non-NPF days over the entire observation period are presented in Fig. 3. For these days, Eq. (2) calculates the difference in the fitting results, with fitting degrees being better on non-NPF days and relatively worse on NPF days. This reflects the fact that $f(\mathrm{RH})$ on NPF days was influenced by more complex factors than on non-NPF days, including the source, composition, and morphology of the aerosols. The fitted $f(\mathrm{RH})$ curve shown in Fig. 3a is apparently below that shown in Fig. 3b. Similarly, both the observed $f(80\,\%)$ and the simulated $f(80\,\%)$ on the NPF days were lower compared to those on the non-NPF days. The $b$ was lower for the NPF days, indicating that the aerosol hygroscopicity of the NPF days was weaker than those of non-NPF days. In this work, $b$ was lower than that in the study done by Zhao et al. (2019b) but slightly higher than the findings of Chen et al. (2014) (Table S4), even though both of their studies were conducted in the North China Plain (NCP), where $PM_{2.5}$ concentrations and $f(\mathrm{RH})$ were higher than those in Xiamen. Due to the proximity of $a$, a smaller $b$ value resulted in the $f(\mathrm{RH})$ being lower in this study compared to those in the NCP. It should be noted that the aerosol scattering hygroscopic growth does not necessarily weaken even in atmospheric environments with light particle pollution. This also shows that aerosol scattering hygroscopic growth is mainly controlled by the aerosol

properties, such as aerosol chemical composition, which are strongly related to the particle formation mechanism and the source of fine particles (Li et al., 2021; Chen et al., 2022a).

### 3.3 Distribution characteristics of $f$(RH) and aerosol chemical compositions

The mass concentrations of the chemical components in NR-$PM_1$ (nonrefractory submicron particles), including $SO_4$, $NO_3$, $NH_4$, Chl and Org, and BC in aerosols, are displayed in Table S5. $SO_4$, $NO_3$, and $NH_4$ (SNA) constituted the majority of the inorganic ions, which were converted from gaseous precursors by complex chemical processes in the atmosphere. Compared to 10 years ago, the concentrations of all SNA in Xiamen have significantly decreased (Deng et al., 2016). The decline ratio in sulfate concentration reached 84.0 %, indicating the effectiveness of sulfate control measures in recent years. In Xiamen, the main measures to control sulfate include the application of desulfurization technology in the flue gas of power plants and coal combustion boilers, as well as the promotion of clean energy for sea ships. However, in contrast to the studies in 2011–2013 and 2017 (Wu et al., 2015a, 2020), the ratio of nitrate to sulfate had increased in this study, suggesting that nitrate pollution has become more prominent in recent years. The concentration of Org decreased in comparison to the previous study, while its proportion in aerosol remained unchanged (Chen et al., 2022b). Additionally, BC is regarded as a hydrophobic species (Zieger et al., 2014).

The diurnal variation in $f$(80 %) and chemical mass fractions are displayed in Fig. 4. The diurnal variation in $f$(RH) was significantly related to the mass fraction of chemical components in particles. NPF days had obviously lower values of $f$(80 %) compared to the other event. The mass concentration of $PM_1$ on the non-NPF days (12.00 $\mu g\,m^{-3}$) was slightly lower than those on the NPF days (12.40 $\mu g\,m^{-3}$). The mass fraction of Org in the aerosol was higher during the NPF period than during the non-NPF period, and $f$(80 %) in the NPF period was smaller than that in the non-NPF period. Based on the wind direction and the homology of Org with BC and CO (Figs. S7, S8), the increasing fraction of Org might be attributed to the emissions from heavy trucks on the major roads near the observation site, which had a weaker impact on the aerosol hygroscopic growth than the SNA.

The $f$(80 %) showed the same pattern as the mass fraction of SNA, especially for nitrate, and the amount of nitrate was significantly low during the NPF period. The mass fraction of sulfate was much higher than that of nitrate on NPF days compared to non-NPF days. The $SO_2$ concentrations on NPF days were clearly higher than those on non-NPF days (Fig. S9). Moreover, $SO_2$ concentrations increased from the morning and peaked around 15:00 (GMT+8) on NPF days, which was consistent with the increasing trend of particle number concentration on NPF days. The reaction of $SO_2$ and OH radicals is considered the primary pathway of sulfuric acid generation (Sipilä et al., 2010). Condensation mode reactions could occur due to the large amount of sulfuric acid in the atmosphere during NPF events. It is hypothesized that condensation mode reactions occurring simultaneously with NPF events were mainly responsible for the higher mass fraction of sulfate during NPF days observed at our site (Yue et al., 2010). Note that the lower $f$(80 %) in the NPF period was probably attributed to the low mass fraction of nitrate and high mass fraction of sulfate in SNA. Chen et al. (2022a) reported that aerosol hygroscopic growth in Shanghai and Guangzhou during NPF days was lower than that during non-NPF days, which was consistent with the results of this study, but the opposite pattern occurred in the NCP. This illuminates that aerosols had a lower hygroscopicity during the NPF event in Xiamen. The study by Liu et al. (2021) also found that the hygroscopicity of 40 nm organic aerosol (OA) was significantly enhanced during NPF days in urban Beijing, which could be derived from different precursors and accounted for the formation of OA during the NPF process. On the basis of aerosol chemical compositions during NPF, it could be speculated that when particle formation occurs on NPF days, the condensation of large quantities of sulfuric acid and organic vapors onto the pre-existing particles results in the conversion of a mixed state on the surface of particles from an external mixture to an internal mixture. These processes alter the optical and chemical properties of particles, which in turn might change the aerosol scattering hygroscopicity growth (Wu et al., 2016).

The sulfur / nitrogen oxidation ratios (SOR/NOR) used to assess the extent of secondary sulfate and nitrate formation are shown in Fig. 5, which were calculated from the formulas of $NOR = [NO_3] / ([NO_3] + [NO_2])$ and $SOR = [SO_4] / ([SO_4] + [SO_2])$, respectively (Liu et al., 2020b). The levels of SOR and NOR were subjected to the regulation by photochemical reactions, exhibiting an increase during daytime. Moreover, the variations in SOR/NOR levels and $f$(80 %) across NPF days were found to be coincident, as SOR/NOR levels dropped down, particularly for NOR, $f$(80 %) also displayed a low level. We assume that nitrate was essential for aerosol scattering and hygroscopic growth. This assumption was confirmed by comparing Fig. 4a and c with Fig. 5a, which shows a significant decline in $f$(RH) when both nitrate content and NOR were low, especially during NPF days. The sharp rise in NOR in the afternoon during the NPF days resulted in an significant increase in the relative amount of nitrate in the aerosol and $f$(80 %), indicating the rapid response of the aerosol hygroscopic growth to nitrate, which can be interpreted as stronger hygroscopicity of nitrate compared to sulfate. On non-NPF days, SOR and NOR were enhanced compared to NPF days, which might be a result of the aqueous-phase reaction at relatively high RH (Sun et al., 2013; Ge et al., 2012). On non-NPF days with high RH and $f$(RH), water vapor condensed onto the particles, and aerosol hygroscopic growth occurred

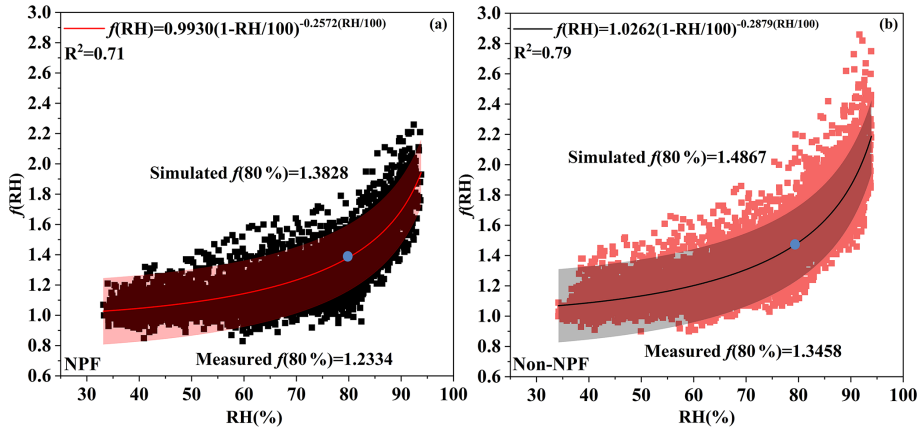


**Figure 3.** The $f(\mathrm{RH})$ curves fitted by Eq. (1) on NPF **(a)** and non-NPF days **(b)**. Red and black lines are the curves fitted by Eq. (2), and blue dots represent the simulated values of $f(80\,\%)$. The light-color shaded areas show the 95 % prediction bands for the fits.

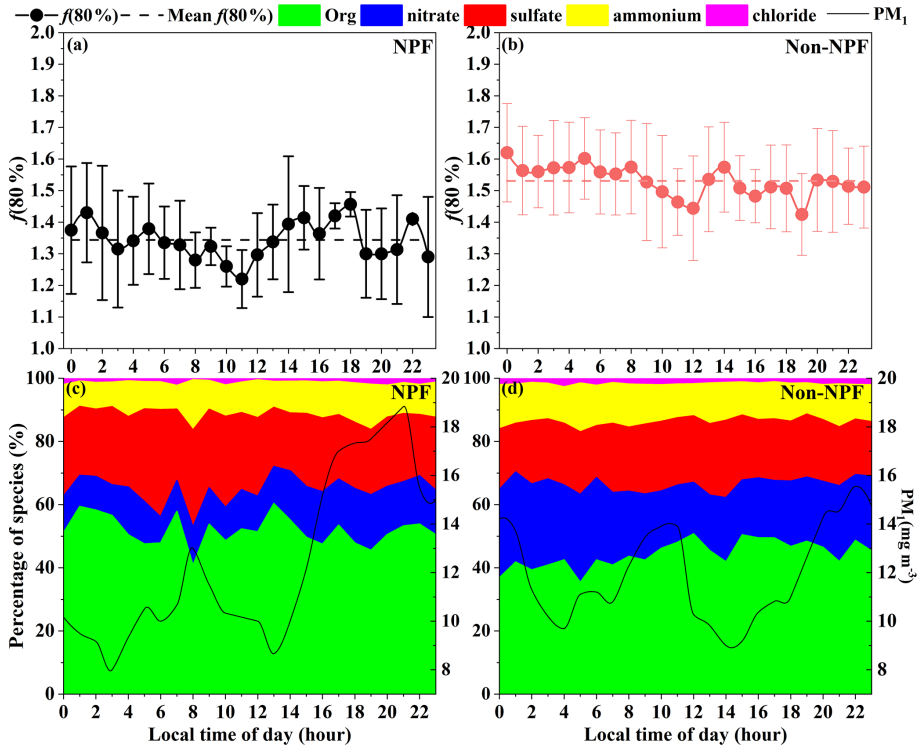


**Figure 4.** Diurnal variations in $f(80\,\%)$ and aerosol chemical mass fractions on NPF and non-NPF days. Panels **(a)** and **(c)** are NPF days and panels **(b)** and **(d)** non-NPF days. These chemical compositions include Org, $NO_3$, $SO_4$, $NH_4$, and Chl. Solid lines are the mass concentrations of $PM_1$; dashed lines are the mean values of $f(80\,\%)$.

(Martin, 2000). The increase in aerosol liquid water content (ALWC) on the surface of particles is crucial for heterogeneous reactions in the atmosphere (Mogili et al., 2006). The heterogeneous hydrolysis of $N_2O_5$ (Pathak et al., 2009; Brown et al., 2005) and the aqueous-phase oxidation of $SO_2$ (Seinfeld et al., 1998; Sun et al., 2013) are important pathways for nitrate and sulfate formation, respectively. In other words, aqueous-phase reactions contribute to the production of secondary aerosol (Ge et al., 2012; Xu et al., 2017a). Thus, the elevation of RH during non-NPF days might promote the transformation of $NO_2$ and $SO_2$ to nitrate and sulfate via aqueous-phase reactions, manifesting as the enhancement of NOR and SOR.

In brief, the influence of SNA on $f(\mathrm{RH})$, particularly nitrate, is significant. Sulfate dominated the SNA during the NPF days, characterized by weaker aerosol hygroscopic

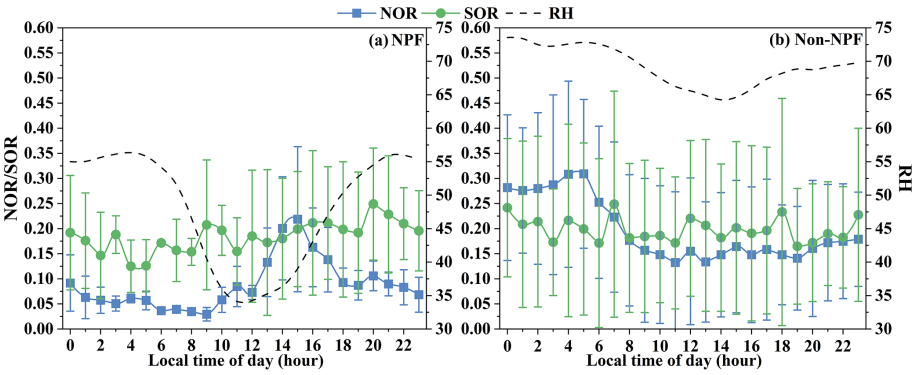


**Figure 5.** Diurnal variations in NOR, SOR, and RH on NPF and non-NPF days. Panel **(a)** denotes NPF days, and panel **(b)** denotes non-NPF days. Blue represents NOR; green represents SOR; dashed lines are RH.

growth compared to non-NPF days, indicating the remarkably different bulk aerosol compositions and condensation mode of aerosol formation mechanisms between NPF and non-NPF days.

### 3.4 Relationships between $f$(RH) and aerosol chemical compositions

Figures 6 and 7 exhibit $f(80\,\%)$ as a function of the mass fractions of SNA and Org between NPF and non-NPF days, revealing the effect of chemical compositions on the aerosol scattering hygroscopic growth. The SNA fraction showed a positive correlation with $f(80\,\%)$ as a result of its high hygroscopicity, whereas the Org fraction demonstrated a negative correlation with $f(80\,\%)$ due to its relatively lower hygroscopicity compared to SNA, in line with findings from previous studies (Zhang et al., 2015; Wu et al., 2017; Ren et al., 2021; Zieger et al., 2014). The magnitude of $R$ for the linear regression was higher during the NPF period compared to the non-NPF period, illuminating a stronger correlation between $f(80\,\%)$ and the mass fraction of SNA or Org specifically during NPF days. The proportion of aerosol chemical compositions remained relatively stable during the non-NPF days, which could account for the limited correlation between $f(80\,\%)$ and their mass fractions during this period. Comparing Fig. 6a and b with Fig. 7a and b, there was a stronger relationship between mass fraction of sulfate and $f(80\,\%)$ on NPF days. Conversely, a stronger association of $f(80\,\%)$ with nitrate was observed on non-NPF days. This indicated that sulfate had an important influence on the aerosol hygroscopicity enhancement during NPF periods, while nitrate was the primary contributor for non-NPF days. This phenomenon could be explained by the fact that the mass fraction of sulfate in the SNA was highest when the NPF event occurred, yet the differences between the mass fractions of sulfate and nitrate were slight on non-NPF days. The role of nitrate in the aerosol hygroscopic properties will be discussed in the following paragraphs.

As mentioned above, the aerosol hygroscopic growth was significantly influenced by the proportion of SNA and Org in aerosols. The fitting parameter $\gamma$, which depends on the aerosol hygroscopicity, is defined as $\gamma = \ln f(\mathrm{RH})/\ln((100/\mathrm{RH_{ref}})/(100-\mathrm{RH}))$ (Quinn et al., 2005; Zhang et al., 2015). Here $\gamma$ was based on $\mathrm{RH_{ref}} = 40\,\%$ and $\mathrm{RH} = 80\,\%$. $\gamma$ can be employed to characterize the relationship between aerosol hygroscopic growth and SNA. The relative quantity of Org and inorganic matters can be expressed as $F_\mathrm{o} = \mathrm{Org}/(\mathrm{Org} + C_i)$, where $C_i$ is the mass concentration of SNA. We chose $NO_3$, $SO_4$, and $NO_3 + SO_4$ as different SNAs constituted in this study, respectively. $\gamma$ and $F_\mathrm{o}$ were negatively correlated for all scatterplots, and linear regressions of $\gamma$ versus $F_\mathrm{o}$ were fitted (Fig. 8). $\gamma$ and $F_\mathrm{o} = \mathrm{Org}/(\mathrm{Org}+\mathrm{NO_3})$ (abbreviated as $F_{\mathrm{o+N}}$, Fig. 8a, d) were more strongly correlated than $\gamma$ and $F_\mathrm{o} = \mathrm{Org}/(\mathrm{Org} + \mathrm{SO_4})$ (abbreviated as $F_{\mathrm{o+S}}$, Fig. 8b, e). Additionally, the correlation between $\gamma$ and $F_\mathrm{o} = \mathrm{Org}/(\mathrm{Org} + \mathrm{NO_3} + \mathrm{SO_4})$ (abbreviated as $F_{\mathrm{o+N+S}}$, Fig. 8c, f) was observed to be smaller than that of the correlation between $\gamma$ and $F_{\mathrm{o+N}}$. This is yet more evidence that $NO_3$ played a more important role than $SO_4$ in determining the aerosol hygroscopicity in Xiamen, contrary to the conclusion of Quinn et al. (2005), Malm et al. (2005), and Yan et al. (2009). These findings also underscored the substantial impact of nitrate on aerosol properties, aligning with recent research conducted in various regions of China (Zhang et al., 2015; Sun et al., 2020; Liao et al., 2020; Jin et al., 2022).

Over the recent decades, the Chinese government has attached great importance to air pollution control, and prominent results have been successful in reducing $SO_2$ emissions (Zhang et al., 2019; Zheng et al., 2018). As the concentration of $SO_2$ decreases, there might be an increasing trend for $NH_3$ to combine with $NO_3^-$ to form $NH_4NO_3$, thereby enhancing the role of nitrate in atmospheric processes. The relatively low value of $f(80\,\%)$ for NPF days can be explained by the fact that the organic and inorganic aerosol fractions were distinct, with sulfate being the predominant

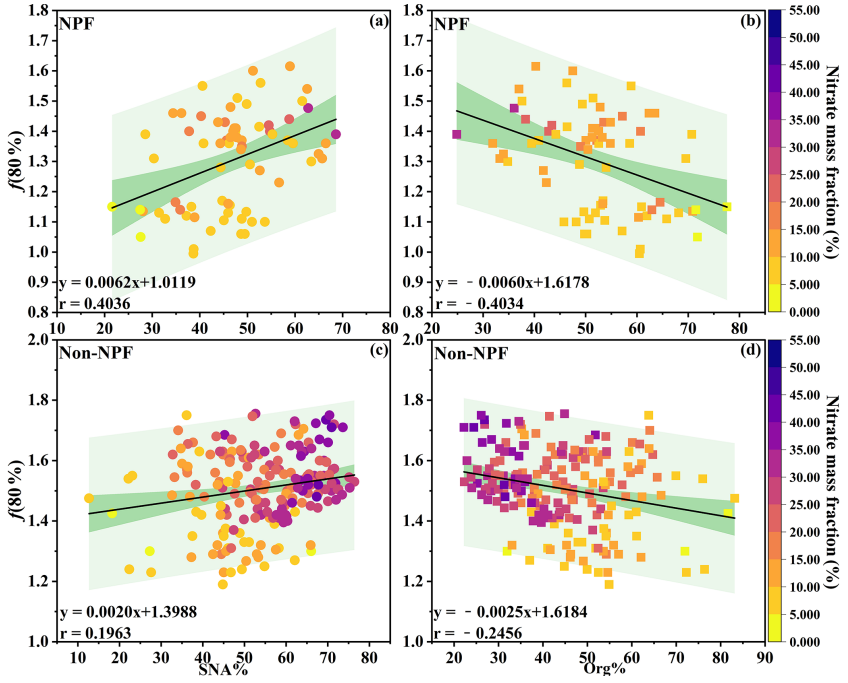


**Figure 6.** The aerosol scattering hygroscopic growth factor $f(80\,\%)$ as a function of SNA and Org mass fraction colored by the nitrate mass fraction. Panels **(a)** and **(b)** denote NPF days; **(c)** and **(d)** denote non-NPF days. The linear regression function and Pearson's correlation coefficient ($R$) are given in each panel. The dark-color shaded areas denote 95 % confidence levels, and the light-color shaded areas show the 95 % prediction bands for the fits.

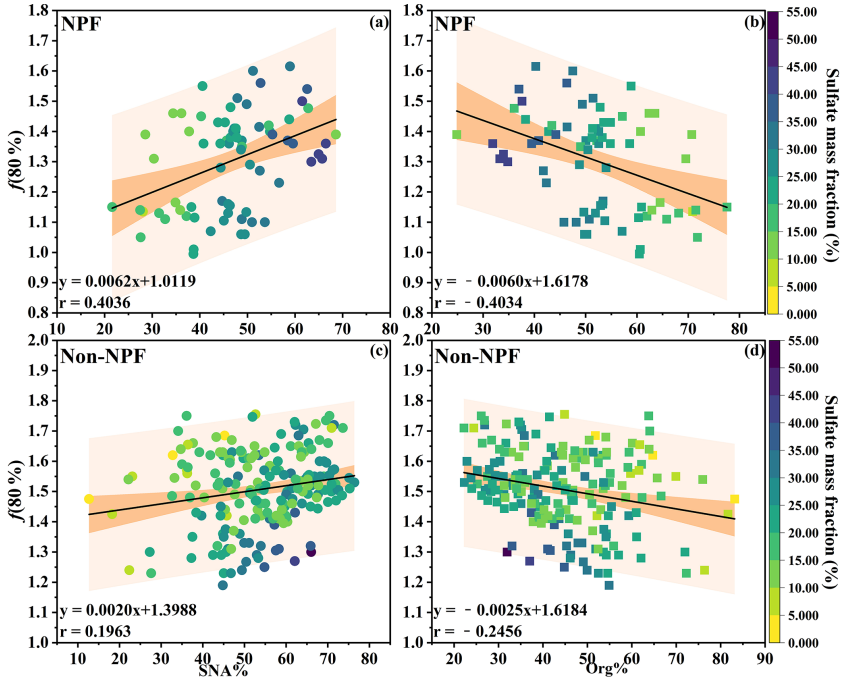


**Figure 7.** The aerosol scattering hygroscopic growth factor $f(80\,\%)$ as a function of SNA and Org mass fraction colored by the sulfate mass fraction. Panels **(a)** and **(b)** denote NPF days; **(c)** and **(d)** denote non-NPF days. The linear regression function and Pearson's correlation coefficient ($R$) are given in each panel. The dark-color shaded areas denote 95 % confidence levels, and the light-color shaded areas show the 95 % prediction bands for the fits.

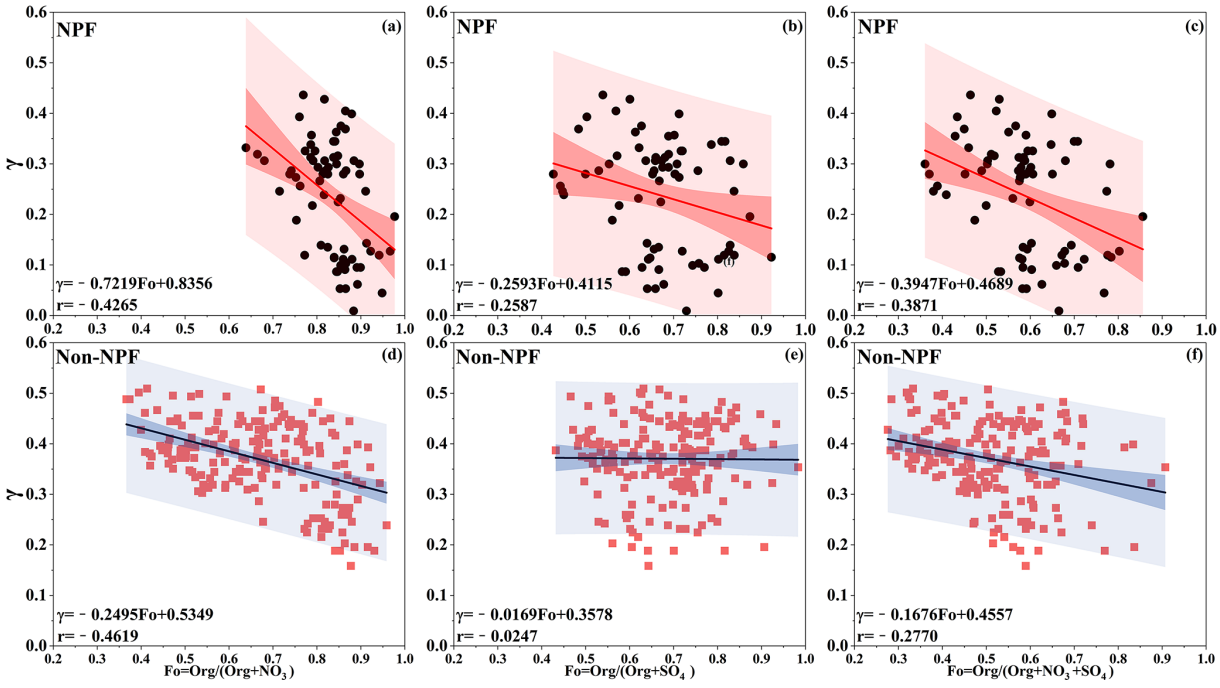


**Figure 8.** Scatterplots of $\gamma$ versus the relative amount of Org and inorganics ($F_o$). **(a, d)** $F_o = \mathrm{Org}/(\mathrm{Org}+\mathrm{NO_3})$, **(b, e)** $F_o = \mathrm{Org}/(\mathrm{Org}+\mathrm{SO_4})$, and **(c, f)** $F_o = \mathrm{Org}/(\mathrm{Org}+\mathrm{NO_3}+\mathrm{SO_4})$. Panels **(a)**, **(b)**, and **(c)** denote the NPF event; **(d)**, **(e)**, and **(f)** denote the non-NPF event. Solid lines represent the linear fit. The dark-color shaded areas denote 95 % confidence levels, and the light-color shaded areas show the 95 % prediction bands for the fits.

component of the inorganic aerosol during this period. During NPF days, there was a stronger correlation between $\gamma$ and $F_{o+S}$, while the correlation between $\gamma$ and $F_{o+S}$ was extremely weak on non-NPF days, which could be related to the role of sulfuric acid in atmospheric nucleation on NPF days. Li et al. (2021) proposed the parameterization of $\gamma$ according to its linear relationship between $F$ and total carbon (TC), and the $R^2$ was 0.92, where $F$ was determined as the mass ratio of $F = \mathrm{TC}/(\mathrm{TC}+\mathrm{NO_3^-}+\mathrm{SO_4^{2-}}+\mathrm{NH_4^+})$. However, the correlation between $\gamma$ and $F_{o+N+S}$ in this study was lower than that reported by Li et al. (2021). As the comparison with these parameterizations suggested, the comprehensive chemical composition information was likely in favor of accurate $\gamma$ parameterizations and subsequent $f(\mathrm{RH})$ determinations.

Overall, SNAs are more effective in promoting aerosol hygroscopic growth than that of Org, with nitrate having the strongest impact.

### 3.5 Aerosol hygroscopicity–chemical composition closure

The hygroscopicity parameter $\kappa$ serves as a highly effective parameter for investigating aerosol hygroscopicity and can be assessed using the humidified nephelometer systems for aerosol light scattering hygroscopic growth factors. The $\kappa_{f(\mathrm{RH})}$, obtained from the measured aerosol scattering hygroscopic growth factor, is a function of the overall hygroscopicity of aerosol particles (Chen et al., 2014; Kuang et al., 2017, 2020) and is widely used to explain the influence of aerosol hygroscopic growth on aerosol optical properties (Tao et al., 2014; Kuang et al., 2015; Brock et al., 2016). Moreover, $\kappa$ can be estimated based on the mass concentration and chemical composition of particles, commonly known as $\kappa_{\mathrm{chem}}$. According to Kuang et al. (2020), $\kappa_{f(\mathrm{RH})}$ accurately represents $\kappa_{\mathrm{chem}}$ and can therefore be used for the aerosol hygroscopicity–chemistry composition closure, which was used to investigate the effect of aerosol chemical composition on the overall aerosol hygroscopicity in this study. The average $\kappa_{f(\mathrm{RH})}$ from 60 % to 90 % was used as a proxy for hygroscopicity closure.

Figure 9 shows the contribution of chemical composition to $\kappa_{f(\mathrm{RH})}$, calculated as the product of $\kappa$ and its volume fraction for each aerosol chemical composition. During the observation period, the inorganic salts, especially SNAs, played a major role in the aerosol hygroscopicity, while some previous studies found that low water-soluble compounds, most likely secondary organic species, predominantly promote new particle formation and have an effect on aerosol hygroscopicity and their cloud condensation nuclei (CCN) activity (Levin et al., 2012; Wu et al., 2015b; Väkevä et al., 2002). For aerosol hygroscopicity during NPF days, $\mathrm{NH_4HSO_4}$ (ABS) was the most dominant contributor, followed by $\mathrm{NH_4NO_3}$ (AN). Although $(\mathrm{NH_4})_2\mathrm{SO_4}$ (AS) ranked third place to aerosol hygroscopicity in NPF, it was still

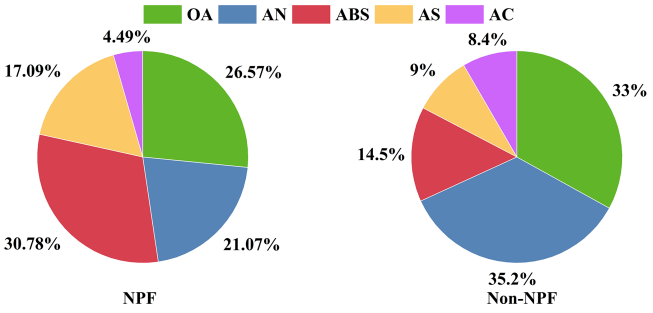


**Figure 9.** Contribution of aerosol chemical composition to $\kappa_{f(\mathrm{RH})}$ on NPF and non-NPF days. Green, blue, red, yellow, and purple code represent organic aerosol (OA), $NH_4NO_3$ (AN), $NH_4HSO_4$ (ABS), $(NH_4)_2SO_4$ (AS), and $NH_4Cl$ (AC), respectively.

higher than its contributions to non-NPF days, which was consistent with what we mentioned above: that sulfate was the main factor influencing the aerosol scattering hygroscopicity growth during NPF periods. The contribution of AN to aerosol hygroscopicity was predominant during non-NPF days, while the contribution of AS and ABS decreased substantially compared to those during NPF. The facilitation of organic aerosol (OA) to the aerosol hygroscopicity fluctuated considerably due to variations in OA composition under different events. The 26.57 % of $\kappa_{f(\mathrm{RH})}$ attributed to OA in NPF was lower than that on non-NPF days. This phenomenon was probably associated with the variety of OA components, for instance secondary organic aerosols (SOAs) exhibiting limited hygroscopicity (Wang et al., 2024). Furthermore, during non-NPF days, despite the increased contribution of OA to $\kappa_{f(\mathrm{RH})}$, $f(\mathrm{RH})$ was higher than that of NPF days, which might be related to the increase in the overall aerosol hygroscopicity during this period and the change in physical properties of particles during these days (Wu et al., 2016).

Due to the uncertainty in the hygroscopicity of OA, we investigated the characteristics of the hygroscopicity parameter $\kappa_{\mathrm{OA}}$ for organic aerosol, as well as the relationship between $\kappa_{\mathrm{OA}}$ and the oxidative properties of OA (Fig. 10). Non-NPF days had the highest value of $\kappa_{\mathrm{OA}}$, and NPF days had the lowest. The $\kappa_{\mathrm{OA}}$ values were greater than those of the previous study in China (Wu et al., 2016; Kuang et al., 2020, 2021) but similar to the findings of Chang et al. (2010) at a rural site in Ontario, Canada (Table 1). The proportion of POA and SOA in OA in our study (Fig. S11) showed higher SOA mass fractions on non-NPF days than on NPF days. It is evident that high SOA mass fractions on non-NPF days corresponded to high $\kappa_{\mathrm{OA}}$ values. The results from these previous studies (Wu et al., 2016; Kuang et al., 2020, 2021; Chang et al., 2010) also highlighted that SOA and oxygenated organic aerosols were likely to be the determinants of $\kappa_{\mathrm{OA}}$. Furthermore, SOA dominated OA mass both in this study and previous studies; however, $\kappa_{\mathrm{OA}}$ values differed much across studies. Noted that the hygroscopicity of SOA might vary significantly under different emission and atmospheric conditions due to variations in volatile organic compound (VOC) precursors and SOA formation pathways (Kuang et al., 2021). The discrepancy in $\kappa_{\mathrm{OA}}$ suggests that using a constant $\kappa_{\mathrm{OA}}$ value to calculate $\kappa$ might lead to a large bias.

To further investigate the factors affecting $\kappa_{\mathrm{OA}}$, we compared the effect of OA oxidation level on $\kappa_{\mathrm{OA}}$, where $f_{44}$ was used to represent the level of OA oxidation (Kuang et al., 2020; Chen et al., 2017). The values of $f_{44}$ in the component mass spectrometry were the ratio of $m/z$ 44 to total signals, reflecting the absolute oxidation degree of aerosols (Chen et al., 2022b). The results showed a slightly weak correlation between $\kappa_{\mathrm{OA}}$ and the oxidation level of OA, indicating that the degree of oxidation was one of significant parameters in determining the hygroscopicity of OA. For both NPF days and non-NPF days, the hygroscopicity of OA enhanced with its oxidation level. Most of the previous studies on $\kappa_{\mathrm{OA}}$ had shown that the hygroscopicity of OA usually increased with the uplift of oxidation degree of OA, which was also found in this study. Nevertheless, a more pronounced increase in $\kappa_{\mathrm{OA}}$ with elevated $f_{44}$ was observed on non-NPF days, attributing to the OA components, formation mechanisms, and the species of VOCs among different events, which can also be accounted for by the fact that less hygroscopic OA is produced during the NPF process in Xiamen, in contrast with the finding of Liu et al. (2021). Thereby, it could be found that alterations in the component and oxidation of OA might regulate the variation in $\kappa_{\mathrm{OA}}$ (Timonen et al., 2013; Xu et al., 2014, 2017b). In addition, the $\kappa_{\mathrm{OA}}$ values on NPF and non-NPF days were lower than those in the studies of Chen et al. (2017), Liu et al. (2021), and Kuang et al. (2020). These results reflect that the use of parameters related to oxidative properties, such as $f_{44}$ or the ratio of O and C, alone is not sufficient to characterize the hygroscopicity of OA and that the molecular information of OA and the special formation mechanisms should also be considered (Liu et al., 2021). However, the OA component is still one of the main driving forces of the variation in aerosol hygroscopicity.

## 4 Conclusions

In this study, the aerosol scattering hygroscopic growth during new particle formation in Xiamen, a coastal city in Southeast China, was clearly depicted by in situ observations. The distinct aerosol hygroscopic behaviors were evident during NPF events in the urban environment characterized by the elevated ambient temperatures, high levels of relative humidity, and low pollution. The aerosol scattering hygroscopic growth of NPF days was weaker than those of non-NPF days. However, under high RH conditions (80 % to 90 %), the $f(\mathrm{RH})$ growth of NPF days exceeded that of non-NPF days. Furthermore, it was determined that one of the two-parameter fitting equations was more adept at accurately representing the observed $f(\mathrm{RH})$.

**Table 1.** Comparisons of the average $\kappa_{OA}$ in different studies.

| Study area | Periods | Remarks | Mean $\kappa_{OA}$ | Reference |
|---|---|---|---|---|
| Beijing, China | summer 2014 | urban | 0.06 | Wu et al. (2016) |
| Dingxing, China | 11 Nov–24 Dec 2018 | rural | $0.08 \pm 0.06$ | Kuang et al. (2020) |
| Heshan, China | 30 Sep–17 Nov 2018 | rural | $0.085 \pm 0.05$ | Kuang et al. (2021) |
| Ontario, Canada | spring 2007 | rural | $0.22 \pm 0.04$ | Chang et al. (2010) |
| Xiamen, China | Feb–Apr 2022 | urban | $0.13 \pm 0.11$ (NPF)<br>$0.19 \pm 0.21$ (non-NPF) | this study |

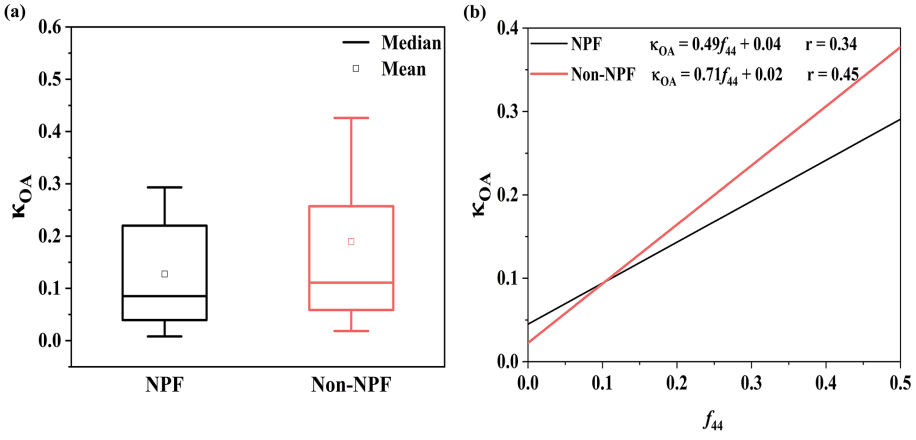


**Figure 10.** The derived $\kappa_{OA}$ and $f_{44}$ on NPF and non-NPF days. **(a)** Variation in $\kappa_{OA}$ between NPF and non-NPF days. **(b)** The relationship between derived $\kappa_{OA}$ and $f_{44}$.

The notable variations in $f(\mathrm{RH})$ between NPF and non-NPF days were impacted by changes in SNA and Org of aerosols. SNA had a more important effect on $f(\mathrm{RH})$ and a higher efficacy in enhancing aerosol hygroscopic growth than that of Org, with nitrate exhibiting the most pronounced impact. Sulfate was highlighted as the dominance in SNA during NPF days, with weaker $f(\mathrm{RH})$ compared to non-NPF days. It is likely that the condensation mode reactions occurring simultaneously with NPF events changed the aerosol chemical composition and had an obvious effect on $f(\mathrm{RH})$. The contribution of SNA to aerosol hygroscopicity surpassed that of Org, with ABS and AN dominating on NPF days and non-NPF days, respectively, revealed by the aerosol hygroscopicity–chemical composition closure. The estimated $\kappa_{OA}$ exhibited a decrease on NPF days compared to non-NPF days, and it showed an increase corresponding to the level of OA oxidation on both two types of days. The uncertainty in OA hygroscopicity resulted from variations in its components and oxidation states; however, it was believed to be an important driver of the alteration in aerosol hygroscopicity. The findings in this study may provide a better explanation of aerosol hygroscopicity properties in the coastal city, which could also offer valuable insights into the use of hygroscopic growth factors in the models of air quality and climate change.

**Data availability.** The dataset for this paper can be accessed at https://doi.org/10.5281/zenodo.13756825 (Li et al., 2024).

**Supplement.** The supplement related to this article is available online at https://doi.org/10.5194/acp-25-3669-2025-supplement.

**Author contributions.** ML and JC conceived the conceptual development of the paper. LL made measurements, analyzed the data, and wrote the paper. ML designed the project and conducted the field campaigns. ML, XF, and JC directed the manuscript development and editing. YC carried out measurements. All authors contributed to discussion and review.

**Competing interests.** The contact author has declared that none of the authors has any competing interests.

**Acknowledgements.** We thank our colleagues and students at the AEG Group in IUE, CAS, for their contributions to the maintenance of the measurements, and at BMET for their technical support with the multi-band dual-nephelometer system.

**Financial support.** This work was funded by the National Natural Science Foundation of China (U22A20578), the Science and Technology Department of Fujian Province (2022L3025), the National Key Research and Development Program (2022YFC3700304), the STS Plan Supporting Project of the Chinese Academy of Sciences in Fujian Province (2023T3013), Fujian Provincial Environmental Protection Science & Technology Plan Projects (2023R004), the Fujian Provincial Natural Science Foundation of China (2024J01199), and the Xiamen Atmospheric Environment Observation and Research Station of Fujian Province.

**Review statement.** This paper was edited by Annele Virtanen and reviewed by two anonymous referees.

## References

Baynard, T., Garland, R. M., Ravishankara, A. R., Tolbert, M. A., and Lovejoy, E. R.: Key factors influencing the relative humidity dependence of aerosol light scattering, Geophys. Res. Lett., 33, L06813, https://doi.org/10.1029/2005gl024898, 2006.

Brock, C. A., Wagner, N. L., Anderson, B. E., Attwood, A. R., Beyersdorf, A., Campuzano-Jost, P., Carlton, A. G., Day, D. A., Diskin, G. S., Gordon, T. D., Jimenez, J. L., Lack, D. A., Liao, J., Markovic, M. Z., Middlebrook, A. M., Ng, N. L., Perring, A. E., Richardson, M. S., Schwarz, J. P., Washenfelder, R. A., Welti, A., Xu, L., Ziemba, L. D., and Murphy, D. M.: Aerosol optical properties in the southeastern United States in summer – Part 1: Hygroscopic growth, Atmos. Chem. Phys., 16, 4987–5007, https://doi.org/10.5194/acp-16-4987-2016, 2016.

Brown, S. S., Osthoff, H. D., Stark, H., Dubé, W. P., Ryerson, T. B., Warneke, C., de Gouw, J. A., Wollny, A. G., Parrish, D. D., Fehsenfeld, F. C., and Ravishankara, A. R.: Aircraft observations of daytime $NO_3$ and $N_2O_5$ and their implications for tropospheric chemistry, J. Photochem. Photobio. A, 176, 270–278, https://doi.org/10.1016/j.jphotochem.2005.10.004, 2005.

Carrico, C. M., Kus, P., Rood, M. J., Quinn, P. K., and Bates, T. S.: Mixtures of pollution, dust, sea salt, and volcanic aerosol during ACE-Asia: Radiative properties as a function of relative humidity, J. Geophys. Res.-Atmos., 108, 8650, https://doi.org/10.1029/2003jd003405, 2003.

Chang, R. Y.-W., Slowik, J. G., Shantz, N. C., Vlasenko, A., Liggio, J., Sjostedt, S. J., Leaitch, W. R., and Abbatt, J. P. D.: The hygroscopicity parameter ($\kappa$) of ambient organic aerosol at a field site subject to biogenic and anthropogenic influences: relationship to degree of aerosol oxidation, Atmos. Chem. Phys., 10, 5047–5064, https://doi.org/10.5194/acp-10-5047-2010, 2010.

Charlson, R. J., Schwartz, S. E., Hales, J. M., Cess, R. D., Coakley, J. A., Hansen, J. E., and Hofmann, D. J.: Climate Forcing By Anthropogenic Aerosols, Science, 255, 423–430, https://doi.org/10.1126/science.255.5043.423, 1992.

Chen, G. J., Shi, Q., Xu, L. L., Yu, S. C., Lin, Z. Y., Ji, X. T., Fan, X. L., Hong, Y. W., Li, M. R., Zhang, F. W., Chen, J. F., and Chen, J. S.: Photochemistry in the urban agglomeration along the coastline of southeastern China: Pollution mechanism and control implication, Sci. Total Environ., 901, 166318, https://doi.org/10.1016/j.scitotenv.2023.166318, 2023.

Chen, J., Zhao, C. S., Ma, N., and Yan, P.: Aerosol hygroscopicity parameter derived from the light scattering enhancement factor measurements in the North China Plain, Atmos. Chem. Phys., 14, 8105–8118, https://doi.org/10.5194/acp-14-8105-2014, 2014.

Chen, J., Budisulistiorini, S. H., Itoh, M., Lee, W.-C., Miyakawa, T., Komazaki, Y., Yang, L. D. Q., and Kuwata, M.: Water uptake by fresh Indonesian peat burning particles is limited by water-soluble organic matter, Atmos. Chem. Phys., 17, 11591–11604, https://doi.org/10.5194/acp-17-11591-2017, 2017.

Chen, L., Zhang, F., Zhang, D., Wang, X., Song, W., Liu, J., Ren, J., Jiang, S., Li, X., and Li, Z.: Measurement report: Hygroscopic growth of ambient fine particles measured at five sites in China, Atmos. Chem. Phys., 22, 6773–6786, https://doi.org/10.5194/acp-22-6773-2022, 2022a.

Chen, T. Z., Chu, B. W., Ma, Q. X., Zhang, P., Liu, J., and He, H.: Effect of relative humidity on SOA formation from aromatic hydrocarbons: Implications from the evolution of gas- and particle-phase species, Sci. Total Environ., 773, 145015, https://doi.org/10.1016/j.scitotenv.2021.145015, 2021.

Chen, Y. P., Yang, C., Xu, L. L., Chen, J. S., Zhang, Y. R., Shi, J. Y., Fan, X. L., Zheng, R. H., Hong, Y. W., and Li, M. R.: Chemical composition of NR-PM1 in a coastal city of Southeast China: Temporal variations and formation pathways, Atmos. Environ., 285, 119243, https://doi.org/10.1016/j.atmosenv.2022.119243, 2022b.

Covert, D. S., Charlson, R. J., and Ahlquist, N. C.: A Study of the Relationship of Chemical Composition and Humidity to Light Scattering by Aerosols, J. Appl. Meteorol. Clim., 11, 968–976, https://doi.org/10.1175/1520-0450(1972)011<0968:ASOTRO>2.0.CO;2, 1972.

Dal Maso, M., Kulmala, M., Riipinen, I., Wagner, R., Hussein, T., Aalto, P. P., and Lehtinen, K. E. J.: Formation and growth of fresh atmospheric aerosols: eight years of aerosol size distribution data from SMEAR II, Hyytiala, Finland, Boreal Environ. Res., 10, 323–336, 2005.

Deng, J. J., Zhang, Y. R., Hong, Y. W., Xu, L. L., Chen, Y. T., Du, W. J., and Chen, J. S.: Optical properties of $PM_{2.5}$ and the impacts of chemical compositions in the coastal city Xiamen in China, Sci. Total Environ., 557, 665–675, https://doi.org/10.1016/j.scitotenv.2016.03.143, 2016.

Ding, J., Zhang, Y., Zheng, N., Zhang, H., Yu, Z., Li, L., Yuan, J., Tang, M., and Feng, Y.: Size Distribution of Aerosol Hygroscopic Growth Factors in Winter in Tianjin, Environ. Sci., 42, 574–583, https://doi.org/10.13227/j.hjkx.202007273, 2021 (in Chinese).

Fierz-Schmidhauser, R., Zieger, P., Wehrle, G., Jefferson, A., Ogren, J. A., Baltensperger, U., and Weingartner, E.: Measurement of relative humidity dependent light scattering of aerosols, Atmos. Meas. Tech., 3, 39–50, https://doi.org/10.5194/amt-3-39-2010, 2010a.

Fierz-Schmidhauser, R., Zieger, P., Vaishya, A., Monahan, C., Bialek, J., O'Dowd, C. D., Jennings, S. G., Baltensperger, U., and Weingartner, E.: Light scattering enhancement factors in the marine boundary layer (Mace Head, Ireland), J. Geophys. Res.-Atmos., 115, D20204, https://doi.org/10.1029/2009jd013755, 2010b.

Gasso, S., Hegg, D. A., Covert, D. S., Collins, D., Noone, K. J., Ostrom, E., Schmid, B., Russell, P. B., Livingston, J. M., Durkee, P. A., and Jonsson, H.: Influence of humidity on the aerosol scattering coefficient and its effect on the upwelling radiance during ACE-2, Tellus B, 52, 546–567, https://doi.org/10.1034/j.1600-0889.2000.00055.x, 2000.

Ge, X. L., Zhang, Q., Sun, Y. L., Ruehl, C. R., and Setyan, A.: Effect of aqueous-phase processing on aerosol chemistry and size distributions in Fresno, California, during wintertime, Environ. Chem., 9, 221–235, https://doi.org/10.1071/en11168, 2012.

Giordano, M., Espinoza, C., and Asa-Awuku, A.: Experimentally measured morphology of biomass burning aerosol and its impacts on CCN ability, Atmos. Chem. Phys., 15, 1807–1821, https://doi.org/10.5194/acp-15-1807-2015, 2015.

Guan, X., Wang, M., Du, T., Tian, P. F., Zhang, N. Y., Shi, J. S., Chang, Y., Zhang, L., Zhang, M., Song, X., and Sun, Y. J.: Wintertime aerosol optical properties in Lanzhou, Northwest China: Emphasis on the rapid increase of aerosol absorption under high particulate pollution, Atmos. Environ., 246, 118081, https://doi.org/10.1016/j.atmosenv.2020.118081, 2021.

Gysel, M., Crosier, J., Topping, D. O., Whitehead, J. D., Bower, K. N., Cubison, M. J., Williams, P. I., Flynn, M. J., McFiggans, G. B., and Coe, H.: Closure study between chemical composition and hygroscopic growth of aerosol particles during TORCH2, Atmos. Chem. Phys., 7, 6131–6144, https://doi.org/10.5194/acp-7-6131-2007, 2007.

Holmes, N. S.: A review of particle formation events and growth in the atmosphere in the various environments and discussion of mechanistic implications, Atmos. Environ., 41, 2183–2201, https://doi.org/10.1016/j.atmosenv.2006.10.058, 2007.

IPCC: Climate Change 2021: The Physical Science Basis. Contribution of Working Group I to the Sixth Assessment Report of the Intergovernmental Panel on Climate Change, edited by: Masson-Delmotte, V., Zhai, P., Pirani, A., Connors, S. L., Péan, C., Berger, S., Caud, N., Chen, Y., Goldfarb, L., Gomis, M. I., Huang, M., Leitzell, K., Lonnoy, E., Matthews, J. B. R., Maycock, T. K., Waterfield, T., Yelekçi, O., Yu, R., and Zhou, B., Cambridge University Press, Cambridge, UK, https://doi.org/10.1017/9781009157896, 2021.

Jin, X. A., Li, Z. Q., Wu, T., Wang, Y. Y., Su, T. N., Ren, R. M., Wu, H., Zhang, D. M., Li, S. Z., and Cribb, M.: Differentiating the Contributions of Particle Concentration, Humidity, and Hygroscopicity to Aerosol Light Scattering at Three Sites in China, J. Geophys. Res.-Atmos., 127, e2022JD036891, https://doi.org/10.1029/2022jd036891, 2022.

Kalkavouras, P., BougiatiotI, A., Hussein, T., Kalivitis, N., Stavroulas, I., Michalopoulos, P., and Mihalopoulos, N.: Regional New Particle Formation over the Eastern Mediterranean and Middle East, Atmosphere, 12, 13, https://doi.org/10.3390/atmos12010013, 2021.

Kotchenruther, R. A. and Hobbs, P. V.: Humidification factors of aerosols from biomass burning in Brazil, J. Geophys. Res.-Atmos., 103, 32081–32089, https://doi.org/10.1029/98jd00340, 1998.

Kotchenruther, R. A., Hobbs, P. V., and Hegg, D. A.: Humidification factors for atmospheric aerosols off the mid-Atlantic coast of the United States, J. Geophys. Res.-Atmos., 104, 2239–2251, https://doi.org/10.1029/98jd01751, 1999.

Kreidenweis, S. M. and Asa-Awuku, A.: Aerosol Hygroscopicity: Particle Water Content and Its Role in Atmospheric Processes, Treatise Geochem., 5, 331–361, 2014.

Kuang, Y., Zhao, C. S., Tao, J. C., and Ma, N.: Diurnal variations of aerosol optical properties in the North China Plain and their influences on the estimates of direct aerosol radiative effect, Atmos. Chem. Phys., 15, 5761–5772, https://doi.org/10.5194/acp-15-5761-2015, 2015.

Kuang, Y., Zhao, C., Tao, J., Bian, Y., Ma, N., and Zhao, G.: A novel method for deriving the aerosol hygroscopicity parameter based only on measurements from a humidified nephelometer system, Atmos. Chem. Phys., 17, 6651–6662, https://doi.org/10.5194/acp-17-6651-2017, 2017.

Kuang, Y., He, Y., Xu, W., Zhao, P., Cheng, Y., Zhao, G., Tao, J., Ma, N., Su, H., Zhang, Y., Sun, J., Cheng, P., Yang, W., Zhang, S., Wu, C., Sun, Y., and Zhao, C.: Distinct diurnal variation in organic aerosol hygroscopicity and its relationship with oxygenated organic aerosol, Atmos. Chem. Phys., 20, 865–880, https://doi.org/10.5194/acp-20-865-2020, 2020.

Kuang, Y., Huang, S., Xue, B., Luo, B., Song, Q., Chen, W., Hu, W., Li, W., Zhao, P., Cai, M., Peng, Y., Qi, J., Li, T., Wang, S., Chen, D., Yue, D., Yuan, B., and Shao, M.: Contrasting effects of secondary organic aerosol formations on organic aerosol hygroscopicity, Atmos. Chem. Phys., 21, 10375–10391, https://doi.org/10.5194/acp-21-10375-2021, 2021.

Kulmala, M., Petaja, T., Nieminen, T., Sipila, M., Manninen, H. E., Lehtipalo, K., Dal Maso, M., Aalto, P. P., Junninen, H., Paasonen, P., Riipinen, I., Lehtinen, K. E. J., Laaksonen, A., and Kerminen, V. M.: Measurement of the nucleation of atmospheric aerosol particles, Nat. Protoc., 7, 1651–1667, https://doi.org/10.1038/nprot.2012.091, 2012.

Levin, E. J. T., Prenni, A. J., Petters, M. D., Kreidenweis, S. M., Sullivan, R. C., Atwood, S. A., Ortega, J., DeMott, P. J., and Smith, J. N.: An annual cycle of size-resolved aerosol hygroscopicity at a forested site in Colorado, J. Geophys. Res.-Atmos., 117, D06201, https://doi.org/10.1029/2011jd016854, 2012.

Li, J. W., Zhang, Z. S., Wu, Y. F., Tao, J., Xia, Y. J., Wang, C. Y., and Zhang, R. J.: Effects of chemical compositions in fine particles and their identified sources on hygroscopic growth factor during dry season in urban Guangzhou of South China, Sci. Total Environ., 801, 149749, https://doi.org/10.1016/j.scitotenv.2021.149749, 2021.

Li, L., Li, M., and Chen, J.: Measurement report: The variation properties of aerosol hygroscopic gr owth related to chemical composition during new particle formation days in a coastal city of southeast China, Zenodo [data set], https://doi.org/10.5281/zenodo.13756825, 2024.

Liao, W. J., Zhou, J. B., Zhu, S. J., Xiao, A. S., Li, K., and Schauer, J. J.: Characterization of aerosol chemical compo-

sition and the reconstruction of light extinction coefficients during winter in Wuhan, China, Chemosphere, 241, 125033, https://doi.org/10.1016/j.chemosphere.2019.125033, 2020.

Liu, H. J., Zhao, C. S., Nekat, B., Ma, N., Wiedensohler, A., van Pinxteren, D., Spindler, G., Müller, K., and Herrmann, H.: Aerosol hygroscopicity derived from size-segregated chemical composition and its parameterization in the North China Plain, Atmos. Chem. Phys., 14, 2525–2539, https://doi.org/10.5194/acp-14-2525-2014, 2014.

Liu, J. Y., Ren, C. H., Huang, X., Nie, W., Wang, J. P., Sun, P., Chi, X. G., and Ding, A. J.: Increased Aerosol Extinction Efficiency Hinders Visibility Improvement in Eastern China, Geophys. Res. Lett., 47, e2020GL090167, https://doi.org/10.1029/2020gl090167, 2020a.

Liu, J. Y., Zhang, F., Xu, W. Q., Sun, Y. L., Chen, L., Li, S. Z., Ren, J. Y., Hu, B., Wu, H., and Zhang, R. Y.: Hygroscopicity of Organic Aerosols Linked to Formation Mechanisms, Geophys. Res. Lett., 48, e2020GL091683, https://doi.org/10.1029/2020gl091683, 2021.

Liu, T. T., Hu, B. Y., Yang, Y. X., Li, M. R., Hong, Y. W., Xu, X. B., Xu, L. L., Chen, N. H., Chen, Y. T., Xiao, H., and Chen, J. S.: Characteristics and source apportionment of $PM_{2.5}$ on an island in Southeast China: Impact of sea-salt and monsoon, Atmos. Res., 235, 104786, https://doi.org/10.1016/j.atmosres.2019.104786, 2020b.

Liu, T., Hong, Y., Li, M., Xu, L., Chen, J., Bian, Y., Yang, C., Dan, Y., Zhang, Y., Xue, L., Zhao, M., Huang, Z., and Wang, H.: Atmospheric oxidation capacity and ozone pollution mechanism in a coastal city of southeastern China: analysis of a typical photochemical episode by an observation-based model, Atmos. Chem. Phys., 22, 2173–2190, https://doi.org/10.5194/acp-22-2173-2022, 2022.

Liu, X. and Zhang, Y.: Advances in Research on Aerosol Hygroscopic Properties at Home and Abroad, Climatic and Environmental Research, 15, 808–816, 2010 (in Chinese).

Liu, X. G., Zhang, Y. H., Cheng, Y. F., Hu, M., and Han, T. T.: Aerosol hygroscopicity and its impact on atmospheric visibility and radiative forcing in Guangzhou during the 2006 PRIDE-PRD campaign, Atmos. Environ., 60, 59–67, https://doi.org/10.1016/j.atmosenv.2012.06.016, 2012.

Liu, X. G., Gu, J. W., Li, Y. P., Cheng, Y. F., Qu, Y., Han, T. T., Wang, J. L., Tian, H. Z., Chen, J., and Zhang, Y. H.: Increase of aerosol scattering by hygroscopic growth: Observation, modeling, and implications on visibility, Atmos. Res., 132, 91–101, https://doi.org/10.1016/j.atmosres.2013.04.007, 2013.

Malm, W. C. and Day, D. E.: Estimates of aerosol species scattering characteristics as a function of relative humidity, Atmos. Environ., 35, 2845–2860, https://doi.org/10.1016/s1352-2310(01)00077-2, 2001.

Malm, W. C., Day, D. E., Kreidenweis, S. M., Collett, J. L., Carrico, C., McMeeking, G., and Lee, T.: Hygroscopic properties of an organic-laden aerosol, Atmos. Environ., 39, 4969–4982, https://doi.org/10.1016/j.atmosenv.2005.05.014, 2005.

Martin, S. T.: Phase Transitions of Aqueous Atmospheric Particles, Chem. Rev., 100, 3403–3454, https://doi.org/10.1021/cr990034t, 2000.

Mogili, P. K., Kleiber, P. D., Young, M. A., and Grassian, V. H.: $N_2O_5$ hydrolysis on the components of mineral dust and sea salt aerosol:: Comparison study in an environmental aerosol reaction chamber, Atmos. Environ., 40, 7401–7408, https://doi.org/10.1016/j.atmosenv.2006.06.048, 2006.

Pan, X. L., Yan, P., Tang, J., Ma, J. Z., Wang, Z. F., Gbaguidi, A., and Sun, Y. L.: Observational study of influence of aerosol hygroscopic growth on scattering coefficient over rural area near Beijing mega-city, Atmos. Chem. Phys., 9, 7519–7530, https://doi.org/10.5194/acp-9-7519-2009, 2009.

Pathak, R. K., Wu, W. S., and Wang, T.: Summertime $PM_{2.5}$ ionic species in four major cities of China: nitrate formation in an ammonia-deficient atmosphere, Atmos. Chem. Phys., 9, 1711–1722, https://doi.org/10.5194/acp-9-1711-2009, 2009

Petters, M. D. and Kreidenweis, S. M.: A single parameter representation of hygroscopic growth and cloud condensation nucleus activity, Atmos. Chem. Phys., 7, 1961–1971, https://doi.org/10.5194/acp-7-1961-2007, 2007.

Quinn, P. K., Bates, T. S., Baynard, T., Clarke, A. D., Onasch, T. B., Wang, W., Rood, M. J., Andrews, E., Allan, J., Carrico, C. M., Coffman, D., and Worsnop, D.: Impact of particulate organic matter on the relative humidity dependence of light scattering: A simplified parameterization, Geophys. Res. Lett., 32, L22809, https://doi.org/10.1029/2005gl024322, 2005.

Ren, R., Li, Z., Yan, P., Wang, Y., Wu, H., Cribb, M., Wang, W., Jin, X., Li, Y., and Zhang, D.: Measurement report: The effect of aerosol chemical composition on light scattering due to the hygroscopic swelling effect, Atmos. Chem. Phys., 21, 9977–9994, https://doi.org/10.5194/acp-21-9977-2021, 2021.

Seinfeld, J., Pandis, S., and Noone, K.: Atmospheric Chemistry and Physics: From Air Pollution to Climate Change, Phys. Today, 51, 88–90, 1998.

Shen, X. J., Sun, J. Y., Ma, Q. L., Zhang, Y. M., Zhong, J. T., Yue, Y., Xia, C., Hu, X. Y., Zhang, S. N., and Zhang, X. Y.: Long-term trend of new particle formation events in the Yangtze River Delta, China and its influencing factors: 7-year dataset analysis, Sci. Total Environ., 807, https://doi.org/10.1016/j.scitotenv.2021.150783, 2022.

Sheridan, P. J., Delene, D. J., and Ogren, J. A.: Four years of continuous surface aerosol measurements from the Department of Energy's Atmospheric Radiation Measurement Program Southern Great Plains Cloud and Radiation Testbed site, J. Geophys. Res.-Atmos., 106, 20735–20747, https://doi.org/10.1029/2001jd000785, 2001.

Sheridan, P. J., Jefferson, A., and Ogren, J. A.: Spatial variability of submicrometer aerosol radiative properties over the Indian Ocean during INDOEX, J. Geophys. Res.-Atmos., 107, INX2 10-1–INX2 10-17, https://doi.org/10.1029/2000jd000166, 2002.

Sipilä, M., Berndt, T., Petäjä, T., Brus, D., Vanhanen, J., Stratmann, F., Patokoski, J., Mauldin, R. L., Hyvärinen, A. P., Lihavainen, H., and Kulmala, M.: The Role of Sulfuric Acid in Atmospheric Nucleation, Science, 327, 1243–1246, https://doi.org/10.1126/science.1180315, 2010.

Stevens, R. and Dastoor, A.: A Review of the Representation of Aerosol Mixing State in Atmospheric Models, Atmosphere, 10, 168, https://doi.org/10.3390/atmos10040168, 2019.

Sun, P., Nie, W., Wang, T. Y., Chi, X. G., Huang, X., Xu, Z., Zhu, C. J., Wang, L., Qi, X. M., Zhang, Q., and Ding, A. J.: Impact of air transport and secondary formation on haze pollution in the Yangtze River Delta: In situ online observations in Shanghai and Nanjing, Atmos. Environ., 225, 117350, https://doi.org/10.1016/j.atmosenv.2020.117350, 2020.

Sun, Y. L., Wang, Z. F., Fu, P. Q., Jiang, Q., Yang, T., Li, J., and Ge, X. L.: The impact of relative humidity on aerosol composition and evolution processes during wintertime in Beijing, China, Atmos. Environ., 77, 927–934, https://doi.org/10.1016/j.atmosenv.2013.06.019, 2013.

Tang, I. N.: Chemical and size effects of hygroscopic aerosols on light scattering coefficients, J. Geophys. Res.-Atmos., 101, 19245–19250, https://doi.org/10.1029/96jd03003, 1996.

Tao, J. C., Zhao, C. S., Ma, N., and Liu, P. F.: The impact of aerosol hygroscopic growth on the single-scattering albedo and its application on the $NO_2$ photolysis rate coefficient, Atmos. Chem. Phys., 14, 12055–12067, https://doi.org/10.5194/acp-14-12055-2014, 2014.

Timonen, H., Carbone, S., Aurela, M., Saarnio, K., Saarikoski, S., Ng, N. L., Canagaratna, M. R., Kulmala, M., Kerminen, V. M., Worsnop, D. R., and Hillamo, R.: Characteristics, sources and water-solubility of ambient submicron organic aerosol in springtime in Helsinki, Finland, J. Aerosol Sci., 56, 61–77, https://doi.org/10.1016/j.jaerosci.2012.06.005, 2013.

Titos, G., Lyamani, H., Cazorla, A., Sorribas, M., Foyo-Moreno, I., Wiedensohler, A., and Alados-Arboledas, L.: Study of the relative humidity dependence of aerosol light-scattering in southern Spain, Tellus B, 66, 24536, https://doi.org/10.3402/tellusb.v66.24536, 2014.

Väkevä, M., Hämeri, K., and Aalto, P. P.: Hygroscopic properties of nucleation mode and Aitken mode particles during nucleation bursts and in background air, J. Geophys. Res.-Atmos., 107, 8104, https://doi.org/10.1029/2000jd000176, 2002.

Wang, J., Li, M., Li, L., Zheng, R., Fan, X., Hong, Y., Xu, L., Chen, J., and Hu, B.: Particle number size distribution and new particle formation in Xiamen, the coastal city of Southeast China in wintertime, Sci. Total Environ., 826, 154208, https://doi.org/10.1016/j.scitotenv.2022.154208, 2022.

Wang, M. L., Chen, Y. Q., Fu, H. Y., Qu, X. L., Shen, G. F., Li, B. G., and Zhu, D. Q.: Combined analyses of hygroscopic properties of organic and inorganic components of three representative black carbon samples recovered from pyrolysis, Sci. Total Environ., 771, 145393, https://doi.org/10.1016/j.scitotenv.2021.145393, 2021.

Wang, Y., Li, J., Fang, F., Zhang, P., He, J., Pöhlker, M. L., Henning, S., Tang, C., Jia, H., Wang, Y., Jian, B., Shi, J., and Huang, J.: In-situ observations reveal weak hygroscopicity in the Southern Tibetan Plateau: implications for aerosol activation and indirect effects, npj Clim. Atmos. Sci., 7, 77, https://doi.org/10.1038/s41612-024-00629-x, 2024.

Won, W. S., Oh, R., Lee, W., Ku, S., Su, P. C., and Yoon, Y. J.: Hygroscopic properties of particulate matter and effects of their interactions with weather on visibility, Sci. Rep., 11, 16401, https://doi.org/10.1038/s41598-021-95834-6, 2021.

Wu, S. P., Schwab, J., Yang, B. Y., Zheng, A., and Yuan, C. S.: Two-Years $PM_{2.5}$ Observations at Four Urban Sites along the Coast of Southeastern China, Aerosol Air Qual. Res., 15, 1799–1812, https://doi.org/10.4209/aaqr.2015.05.0363, 2015a.

Wu, S. P., Cai, M. J., Xu, C., Zhang, N., Zhou, J. B., Yan, J. P., Schwab, J. J., and Yuan, C. S.: Chemical nature of $PM_{2.5}$ and $PM_{10}$ in the coastal urban Xiamen, China: Insights into the impacts of shipping emissions and health risk, Atmos. Environ., 227, 117383, https://doi.org/10.1016/j.atmosenv.2020.117383, 2020.

Wu, Y. F., Wang, X. J., Yan, P., Zhang, L. M., Tao, J., Liu, X. Y., Tian, P., Han, Z. W., and Zhang, R. J.: Investigation of hygroscopic growth effect on aerosol scattering coefficient at a rural site in the southern North China Plain, Sci. Total Environ., 599, 76–84, https://doi.org/10.1016/j.scitotenv.2017.04.194, 2017.

Wu, Z. J., Poulain, L., Birmili, W., Größ, J., Niedermeier, N., Wang, Z. B., Herrmann, H., and Wiedensohler, A.: Some insights into the condensing vapors driving new particle growth to CCN sizes on the basis of hygroscopicity measurements, Atmos. Chem. Phys., 15, 13071–13083, https://doi.org/10.5194/acp-15-13071-2015, 2015b.

Wu, Z. J., Zheng, J., Shang, D. J., Du, Z. F., Wu, Y. S., Zeng, L. M., Wiedensohler, A., and Hu, M.: Particle hygroscopicity and its link to chemical composition in the urban atmosphere of Beijing, China, during summertime, Atmos. Chem. Phys., 16, 1123–1138, https://doi.org/10.5194/acp-16-1123-2016, 2016.

Wu, Z. J., Wang, Y., Tan, T. Y., Zhu, Y. S., Li, M. R., Shang, D. J., Wang, H. C., Lu, K. D., Guo, S., Zeng, L. M., and Zhang, Y. H.: Aerosol Liquid Water Driven by Anthropogenic Inorganic Salts: Implying Its Key Role in Haze Formation over the North China Plain, Environ. Sci. Tech. Let., 5, 160–166, https://doi.org/10.1021/acs.estlett.8b00021, 2018.

Xia, C., Sun, J. Y., Qi, X. F., Shen, X. J., Zhong, J. T., Zhang, X. Y., Wang, Y. Q., Zhang, Y. M., and Hu, X. Y.: Observational study of aerosol hygroscopic growth on scattering coefficient in Beijing: A case study in March of 2018, Sci. Total Environ., 685, 239–247, https://doi.org/10.1016/j.scitotenv.2019.05.283, 2019.

Xia, C., Sun, J. Y., Hu, X. Y., Shen, X. J., Zhang, Y. M., Zhang, S. A., Wang, J. L., Liu, Q., Lu, J. Y., Liu, S., and Zhang, X. Y.: Effects of hygroscopicity on aerosol optical properties and direct radiative forcing in Beijing: Based on two-year observations, Sci. Total Environ., 857, 159233, https://doi.org/10.1016/j.scitotenv.2022.159233, 2023.

Xu, L. L., Duan, F. K., He, K. B., Ma, Y. L., Zhu, L. D., Zheng, Y. X., Huang, T., Kimoto, T., Ma, T., Li, H., Ye, S. Q., Yang, S., Sun, Z. L., and Xu, B. Y.: Characteristics of the secondary water-soluble ions in a typical autumn haze in Beijing, Environ. Pollut., 227, 296–305, https://doi.org/10.1016/j.envpol.2017.04.076, 2017a.

Xu, W., Guo, S., Gomez-Hernandez, M., Zamora, M. L., Secrest, J., Marrero-Ortiz, W., Zhang, A. L., Collins, D. R., and Zhang, R. Y.: Cloud forming potential of oligomers relevant to secondary organic aerosols, Geophys. Res. Lett., 41, 6538–6545, https://doi.org/10.1002/2014gl061040, 2014.

Xu, W. Q., Han, T. T., Du, W., Wang, Q. Q., Chen, C., Zhao, J., Zhang, Y. J., Li, J., Fu, P. Q., Wang, Z. F., Worsnop, D. R., and Sun, Y. L.: Effects of Aqueous-Phase and Photochemical Processing on Secondary Organic Aerosol Formation and Evolution in Beijing, China, Environ. Sci. Technol., 51, 762–770, https://doi.org/10.1021/acs.est.6b04498, 2017b.

Yan, P., Pan, X. L., Tang, J., Zhou, X. J., Zhang, R. J., and Zeng, L. M.: Hygroscopic growth of aerosol scattering coefficient: A comparative analysis between urban and suburban sites at winter in Beijing, Particuology, 7, 52–60, https://doi.org/10.1016/j.partic.2008.11.009, 2009.

Yu, Y. L., Zhao, C. S., Kuang, Y., Tao, J. C., Zhao, G., Shen, C. Y., and Xu, W. Y.: A parameterization for the light scattering enhancement factor with aerosol

chemical compositions, Atmos. Environ., 191, 370–377, https://doi.org/10.1016/j.atmosenv.2018.08.016, 2018.

Yue, D. L., Hu, M., Zhang, R. Y., Wang, Z. B., Zheng, J., Wu, Z. J., Wiedensohler, A., He, L. Y., Huang, X. F., and Zhu, T.: The roles of sulfuric acid in new particle formation and growth in the mega-city of Beijing, Atmos. Chem. Phys., 10, 4953–4960, https://doi.org/10.5194/acp-10-4953-2010, 2010.

Zhang, L., Sun, J. Y., Shen, X. J., Zhang, Y. M., Che, H., Ma, Q. L., Zhang, Y. W., Zhang, X. Y., and Ogren, J. A.: Observations of relative humidity effects on aerosol light scattering in the Yangtze River Delta of China, Atmos. Chem. Phys., 15, 8439–8454, https://doi.org/10.5194/acp-15-8439-2015, 2015.

Zhang, Q., Zheng, Y. X., Tong, D., Shao, M., Wang, S. X., Zhang, Y. H., Xu, X. D., Wang, J. N., He, H., Liu, W. Q., Ding, Y. H., Lei, Y., Li, J. H., Wang, Z. F., Zhang, X. Y., Wang, Y. S., Cheng, J., Liu, Y., Shi, Q. R., Yan, L., Geng, G. N., Hong, C. P., Li, M., Liu, F., Zheng, B., Cao, J. J., Ding, A. J., Gao, J., Fu, Q. Y., Huo, J. T., Liu, B. X., Liu, Z. R., Yang, F. M., He, K. B., and Hao, J. M.: Drivers of improved $PM_{2.5}$ air quality in China from 2013 to 2017, P. Natl. Acad. Sci. USA, 116, 24463–24469, https://doi.org/10.1073/pnas.1907956116, 2019.

Zhao, C. S., Yu, Y. L., Kuang, Y., Tao, J. C., and Zhao, G.: Recent Progress of Aerosol Light-scattering Enhancement Factor Studies in China, Adv. Atmos. Sci., 36, 1015–1026, https://doi.org/10.1007/s00376-019-8248-1, 2019a.

Zhao, P. S., Ding, J., Du, X., and Su, J.: High time-resolution measurement of light scattering hygroscopic growth factor in Beijing: A novel method for high relative humidity conditions, Atmos. Environ., 215, 116912, https://doi.org/10.1016/j.atmosenv.2019.116912, 2019b.

Zheng, B., Tong, D., Li, M., Liu, F., Hong, C., Geng, G., Li, H., Li, X., Peng, L., Qi, J., Yan, L., Zhang, Y., Zhao, H., Zheng, Y., He, K., and Zhang, Q.: Trends in China's anthropogenic emissions since 2010 as the consequence of clean air actions, Atmos. Chem. Phys., 18, 14095–14111, https://doi.org/10.5194/acp-18-14095-2018, 2018.

Zieger, P., Fierz-Schmidhauser, R., Gysel, M., Ström, J., Henne, S., Yttri, K. E., Baltensperger, U., and Weingartner, E.: Effects of relative humidity on aerosol light scattering in the Arctic, Atmos. Chem. Phys., 10, 3875–3890, https://doi.org/10.5194/acp-10-3875-2010, 2010.

Zieger, P., Fierz-Schmidhauser, R., Weingartner, E., and Baltensperger, U.: Effects of relative humidity on aerosol light scattering: results from different European sites, Atmos. Chem. Phys., 13, 10609–10631, https://doi.org/10.5194/acp-13-10609-2013, 2013.

Zieger, P., Fierz-Schmidhauser, R., Poulain, L., Muller, T., Birmili, W., Spindler, G., Wiedensohler, A., Baltensperger, U., and Weingartner, E.: Influence of water uptake on the aerosol particle light scattering coefficients of the Central European aerosol, Tellus B, 66, 22716, https://doi.org/10.3402/tellusb.v66.22716, 2014.